Nuclear Instruments and Methods in Physics Research A 614 (2010) 184–195

Contents lists available at ScienceDirect

Nuclear Instruments and Methods in Physics Research A

journal homepage: www.elsevier.com/locate/nima

# Characterization study of silica aerogel for Cherenkov imaging

Y. Sallaz-Damaz [a], L. Derome [a,*], M. Mangin-Brinet [a], M. Loth [a], K. Protasov [a], A. Putze [a], M. Vargas-Trevino [a,1], O. Véziant [a], M. Buénerd [a], A. Menchaca-Rocha [b], E. Belmont [b], M. Vargas-Magaña [b], H. Léon-Vargas [b], A. Ortiz-Velàsquez [b], A. Malinine [c], F. Baraõ [d], R. Pereira [d], T. Bellunato [e], C. Matteuzzi [e], D.L. Perego [e]

[a] LPSC, IN2P3/CNRS, 53 av. des Martyrs, 38026 Grenoble Cedex, France
[b] Instituto de Fisica, UNAM, AP 20-364, Mexico DF, Mexico
[c] University of Maryland, College Park, MD 20742, USA
[d] LIP, Avenida Elias Garcia 14-1, P - 1000 Lisboa, Portugal
[e] Università degli Studi di Milano-Bicocca and INFN, Milano, Italy

ARTICLE INFO

*Article history:*
Received 4 December 2009
Accepted 7 December 2009
Available online 6 January 2010

*Keywords:*
Cherenkov detectors
Ring imaging
Silica aerogels
Refractive index uniformity

ABSTRACT

Different methods to measure the characteristics of silica aerogel tiles used as Cherenkov radiator in the CREAM and AMS experiments have been investigated to optimize the detector performances. The measurement accuracy dictated by the physics objectives on the velocity and charge resolutions set stringent requirements on the aerogel refractive index determination, namely $\Delta n \sim 1.5 \times 10^{-4}$ and $\Delta n \sim 5 \times 10^{-4}$ for the AMS and CREAM imagers, respectively. The matching of such accuracies for this material turned out to be a metrological challenge, and finally led to a full R&D program, to develop an appropriate characterization procedure. Preliminary studies performed with a standard refractive index measurement technique (laser beam deviation by a prism) have revealed a significant systematic index nonuniformity for the AMS tiles at a level ($10^{-3}$), not acceptable considering the aimed accuracy. These large variations were confirmed in a beam test. A second method, mapping the transverse index gradient by deflection of a laser beam entering normally to the tile has then been developed. It is shown that this procedure is suitable to reach the required accuracy, at the price of using both methods combined. The several hundreds of tiles of the radiator plane of the CREAM and AMS Cherenkov imagers were characterized using a simplified procedure, however, appropriate for each case, compromising between the amount of work and the time available. The experimental procedures and set-ups used are described in the text, and the obtained results are reported.



## 1. Introduction

Since the pioneering work of the Los Alamos group more than a decade ago [1], silica aerogel has become a very widely used radiator material in Cherenkov imaging. In its recent applications, detectors have been built to perform velocity $\beta$ measurements for hadron discrimination in high energy accelerator experiments [2,3]. In less common applications, some detectors using silica aerogel aim at both the velocity and charge measurement of nuclear elements [4–6] in embarked cosmic-ray experiments or in heavy ion accelerator experiments. The main reason for this success is the unique range of refractive index of this material, that bridges a large part of the gap between gas radiators and liquid/solid radiators, with values extending from around $n-1 \approx 4 \times 10^{-3}$ up to around $8 \times 10^{-2}$ for good optical quality material. Attempts are being made to reach larger values than this latter maximum [7]. A first generation of aerogel based Cherenkov imagers has been built over the past decade, or is being built (see for examples Refs. [2,4,5,8]), while new R&D programs for aerogel development are being undertaken to improve the optical quality of the material [9].

In this context of continuous development, the currently available high optical quality but hydrophilic aerogels [10] compete with the hydrophobic materials, that have a slightly lesser optical quality but are easier to handle [11]—the latter, however, being available only in smaller dimensions [12].

In a rapidly evolving context of performances, no specific technique was available yet for the systematic investigation of

* Corresponding author. Tel.: +33 476 284 082; fax: +33 476 284 004.
*E-mail address:* derome@lpsc.in2p3.fr (L. Derome).
[1] Current address: Escuela de Ciencias UABJO, Oaxaca de Jurez, Oaxaca, Mexico.

0168-9002/$ - see front matter © 2010 Elsevier B.V. All rights reserved.
doi:10.1016/j.nima.2009.12.029

the refractive index uniformity over the radiator tiles area. In addition, the practical limit on the index measurement accuracy was not known. The appropriate method had then to be developed for the characterization of the aerogel optical properties.

In all these applications, aerogel is used in the form of tiles with sizes up to 20 cm and thickness up to 5 cm for hydrophilic aerogel [13], while the corresponding maximum values are much lesser for the hydrophobic material, namely $\sim$11 and 1.1 cm, respectively [12].

The value of the refractive index $n$ from tile to tile, and the index uniformity inside each tile is a key feature that contributes to the ultimate detector resolution. Ideally, $n$ should be constant through the tile surface. In practice, the refractive index may be highly variable depending on the fabrication technique and thermal processing of the material. This nonuniformity of $n$ is induced by the density variations arising from the thermal processing. In case this nonuniformity of the refractive index is above the accuracy requirements of the project, the map of the mean $n$ value $\langle n \rangle$ across the radiator area (i.e. the local value of $n$ integrated over the tile thickness) needs to be known with the appropriate accuracy.

In the present work, the properties of two types of aerogel tiles have been investigated, with the purpose of matching the resolution requirements dictated by the scientific objectives of the Cherenkov imagers built for two experimental projects in Cosmic-Ray Physics, namely AMS [14,5] and CREAM [15,6]. In both projects, these detectors will provide the measurement of the nuclear cosmic-ray charge, with for AMS, the velocity over a range of momentum. The corresponding requirements, discussed in the next section, involve different features of the counter, namely, the accuracy of photon counting for the charge measurement, and the accuracy of photon hit position determination for the velocity measurement.

Different type of silica aerogel tiles have been tested for AMS and CREAM imagers. Hydrophilic aerogel from Refs. [16,13], referred to as NOVO in the following, and hydrophobic material from Ref. [11], referred to as MATSU below, were used for the former and the latter, respectively. In both cases, the material was available in the form of tiles, with the same large dimensions $11 \times 11\,\mathrm{cm}^2$, with thickness 2.5 and 1.1 cm for NOVO and MATSU, respectively.

The paper reports on the investigation of different methods to perform aerogel index measurements with the required accuracy. A similar study has been performed recently by the LHCb collaboration and reported in Ref. [3], in the same spirit as the present work.

The next section defines the accuracy requirements on the mean index measurements and sets the limits on the acceptable variations of the latter inside the radiator volume. Section 3 presents the preliminary studies performed using a standard refractive index measurement technique (laser beam deviation by a prism). Section 4 reports on a beam test of a tiles sample, while Section 5 describes the successful method of index mapping by means of laser deflection by transverse index gradient. Section 7 reports on some other investigated properties of the silica aerogel tiles. Section 8 summarizes and concludes the report.

## 2. Index accuracy requirements for velocity and charge measurements

For the AMS experiment [5], as well as for CREAM [6], it is required that the imager achieves the charge measurement of the detected nuclei up to $Z \approx 26$, i.e., the Fe region. The AMS imager must in addition perform the particle velocity $\beta$ measurement from the threshold region up to $\gamma \approx 10$, $\gamma$ being the Lorentz factor of the particle, for isotope mass measurement of light elements. For CREAM, the $\gamma$ of the particles ($10^3 \leq \gamma \leq 10^4$) is two orders of magnitudes beyond the above quoted value, the Cherenkov angle is far inside the asymptotic range, and no velocity measurement can be performed with a practicable accuracy. The index variations $\Delta n$ over the radiator area induces a systematic error on the Cherenkov event reconstruction that has to be kept smaller than statistical errors. This requirement becomes particularly difficult to meet for the charge measurements of large $Z$ nuclei since statistical errors are becoming very small in account of the large photon yield.

### 2.1. Index uniformity required by the velocity resolution

The spatial resolution of a proximity focusing Cherenkov imager that determines its velocity resolution includes three contributions: (a) spread of the photon emission point across the tile thickness, (b) chromatic dispersion plus optical aberrations of the radiator, and (c) spatial resolution of the photon detector, i.e., pixel size in the present case. It is assumed here that the other possible contributions such as multiple scattering of particles and surface scattering of Cherenkov photons, are negligible (see Ref. [17] for the latter).

The total spread resulting from these contributions can be written as

$$\sigma_{tot}^2 = \frac{\sigma_{pix}^2}{N-1} + \frac{\sigma_{chrom}^2}{N-1} + \sigma_n^2 + \sigma_t^2 \quad (1)$$

where $\sigma_n$ and $\sigma_t$ are the systematic errors associated to variations of the refractive index $n$ and of the tile thickness $t$, respectively, for a given tile, $N$ being the number of detected photons, and $\sigma_{pix}$ and $\sigma_{chrom}$ the single photon spatial and chromatic dispersions.

Since the velocity measurement aims at the isotope mass separation over a given range of mass, the acceptable variations of the refractive index, transverse to the mean particle trajectory, over a given tile area, should induce a velocity spread smaller than the $\beta$ resolution of the counter for the nominal value of the refractive index and for the maximum charge for which isotopes are separated. For the AMS imager, $^9$Be and $^{10}$Be separation is a major issue and isotope identification must thus be performed efficiently at least up to $Z = 4$. In test beam measurements, the maximum charge for which isotope separation can be performed with the AMS Cherenkov imager was found to be about 6, and the corresponding velocity resolution measured is $\Delta\beta \sim 1.5 \times 10^{-4}$ [17]. The corresponding spread of the refractive index $n$, $\Delta n/n \sim \Delta\beta/\beta$, inside a given tile, must thus be limited to the drastic requirement $\Delta n/n \ll 1.5 \times 10^{-4}$.

### 2.2. Index uniformity required by the charge resolution

The number of detected Cherenkov photons is given by $N = N_0 Z^2 \sin^2\theta d/\cos\tau$, with $N_0$ being the quality factor of the counter, $d$ the thickness of the radiator, $Z$ the charge of the particle, $\theta$ the Cherenkov angle, related to the refractive index $n$ by $\cos\theta = 1/n$, and $\tau$ the incidence angle of the particle on the radiator plane. The spread of the photon yield induced by the radiator material properties then originates both from the nonuniformity of the refractive index through the Cherenkov angle, and from the variation of the radiator thickness. The uncertainty associated with $\tau$ will not be considered here since not related to the radiator features. In the small Cherenkov angle approximation, the relative error on $Z$, ignoring the uncertainty related to the photon detector (see Ref. [18] for a

discussion of this issue), can be written as

$$\frac{\Delta Z}{Z}=\frac{1}{2}\sqrt{\left(\frac{\Delta N}{N}\right)^2+\left(\frac{\Delta(n-1)}{(n-1)}\right)^2+\left(\frac{\Delta d}{d}\right)^2}. \quad (2)$$

The dispersion of the number of produced photons thus depends on the refractive index uniformity across the radiator plane and thereby on the density of the radiator material. In practice, the best experimental $\Delta Z$ measured around the center of the tile with the AMS prototype in beam tests is $\sim 0.25$ charge unit (standard deviation) [17]. Assuming for the moment $d$ to be constant, the dispersion of $n$ due to nonuniformities over the tile volume, must be small enough so as not to deteriorate this experimental value for nuclei up to around $Z=26$, thus $\Delta(n-1)/(n-1) \ll 2\times 10^{-2}$, or $\Delta n \ll 10^{-3}$ for $n\sim 1.05$, the value of refractive index used for both AMS and CREAM Cherenkov imagers.

The contribution to the counter resolution of this transverse variations of $n$ sets the upper limit for the charge separation of nuclear elements, as it can be seen from the examination of relation (2) above. Note also that this requirement on the charge measurement accuracy is less constraining than the velocity resolution requirement for the AMS Cherenkov detector.

### 2.3. Thickness spread

The thickness spread induces a proportional spread of the photon yield and then generates a systematic error that limits the $Z$ accuracy. Relation (2) shows that the thickness uncertainty must be limited to $\Delta d/d \ll 2\times 10^{-2}$. The tile thickness must then be controlled with an accuracy better than about 0.2 mm for the CREAM detector radiator. This is further discussed below for each instrument.

If the above requirements cannot be met inside a given tile, then the detailed index and thickness mapping of each tile has to be performed and used in the data analysis for the detector resolution requirements to be satisfied. The purpose of this study was to check on a significant sample of the radiator material, whether or not these requirements were met. As it will be seen below, this turned out not to be the case, and complete mapping of the tiles should be performed to strictly match the requirements.

## 3. Optical index measurements by the prism method

The first method used was the standard prism method. Straightforward in principle and easy to implement, it is described in many textbooks on optics (see Ref. [19] for example). In the present case, however, some significant limitations arose from the poor optical interfaces degrading the beam quality for numerous tiles, and from the poor angular accuracy of the prism dihedron, nominally of 90°, increasing the uncertainty on the deviation angle.

### 3.1. Principle of the method

This well known method relies on the deviation measurement of a laser beam passing through the tile edges. The adjacent tile sides form a dihedron (prism) and the deviation undergone by the laser when crossing this interface is given by the Snell–Descartes laws:

$$\delta=\alpha-\beta+\arcsin\left\{n\cdot\sin\left[\beta-\arcsin\left(\frac{\sin\alpha}{n}\right)\right]\right\}. \quad (3)$$

Here $n$ is the ratio of the aerogel index $n_{AGL}$ over the air index $n_{air}$, $\beta$ is the prism angle, and $\alpha$ the laser incident angle. Considering the accuracy we would like to achieve (few $10^{-4}$) it is important to take $n_{air}-1=3\times 10^{-4}$. This function (3) has a minimum for $\alpha_{min}=\arcsin(n\cdot\sin(\beta/2))$:

$$\delta_{min}=2\arcsin\left[n\cdot\sin\frac{\beta}{2}\right]-\beta.$$

The tile refractive index can thus be determined by measuring and fitting the angular distribution of the laser deviation obtained from varying the incidence angle $\alpha$.

It must be noted that the method has some practical geometrical limits in the present case since only the regions where a dihedron between two adjacent faces or sides are available for the prism technique to be applicable. These are namely the four tile corners between two adjacent sides, and the eight corners between the two faces and the four side. This limited the measurements to a narrow band along the tile periphery where the technique can be applied, and does not allow the measurement over the entire tile surface. The latter appeared to be as much necessary as significant gradients of index have been measured close to the tiles edges.

### 3.2. Experimental set-up

A schematic view of the experimental set-up used for the measurements is shown in Fig. 1. The angle $\theta$ between the symmetry axis of the prism and the vertical direction is related to the incident angle $\alpha$ by $\theta=\alpha-\pi/4$. The position of the laser beam spot is measured on a screen placed downstream at a distance chosen to match the required accuracy and the direct beam (i.e. without aerogel tile) gives the zero deviation position. The displacement of the spot along the screen induced by refraction in the sample provides, after corrections (see Appendix A), a measurement of the deviation angle $\delta$.

The aerogel sample was softly clamped on a rotary stage. The vertical rotation axis of the table was set to contain the laser spot (Fig. 1), so that it remains at a fixed point on the tile interface when the stage is rotated.

All optical elements were mounted on a dedicated optical bench: laser source (red and blue lasers were available), support stage for aerogel tiles sample, and screen. The support stage was movable in the $(x,y)$ direction in the plane transverse to the beam, to scan the tile edges, and it could rotate around a vertical axis to vary the incidence angle $\theta$ on the sample. The measurement screen was placed about 2.5–3 m downstream in front of a CCD camera interfaced with a computer. This optical ensemble was enclosed in a stand equipped with sliding lateral shutters (see Fig. 2). The $x$, $y$, and $\theta$ movement functions of the tile supporting stage were remotely controlled and entirely automatized, allowing large sets of points to be measured in a few minutes without any intervention of the operator [20]. A red laser (wavelength $\lambda=632.8$ nm) was used for the systematic study,

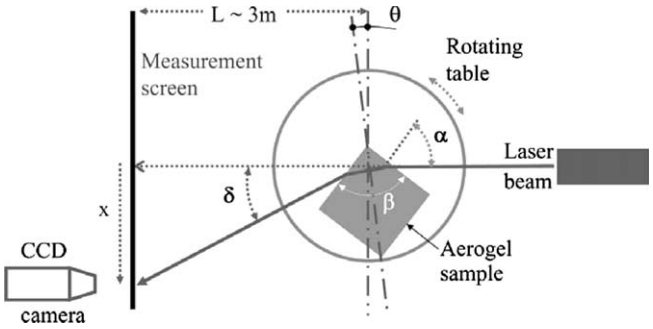


**Fig. 1.** Schematics of the experimental set-up.

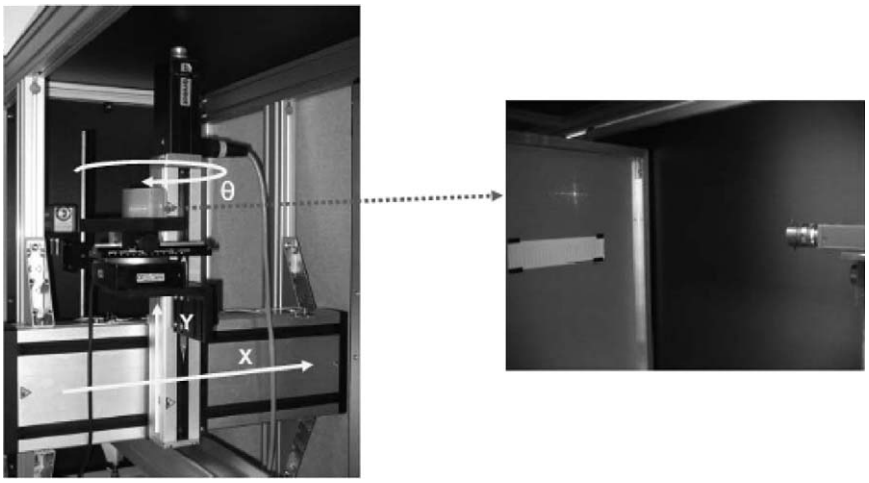


**Fig. 2.** Photographic views of the experimental set-up. Left: laser source, aerogel sample on the $X, Y, \theta$ adjustable support. Right: screen with a laser spot and the CCD camera recording the laser spot deviation.

although measurements using a blue laser would have been more appropriate. Measurements using the latter have been attempted, but turned out to be very difficult due to important Rayleigh scattering in the material. The evaluation of the index value at 420 nm, maximum sensitivity of the photomultiplier tubes (PMTs) of the Cherenkov detectors, was obtained from the measurements using the Lorentz–Lorenz law [21].

The image of the laser beam on the screen seen by the CCD camera was recorded on a PC computer by means of a dedicated data acquisition software based on the LABVIEW environment. The image size was $1024 \times 768$ pixels with 8 bits per color, i.e., 24 bits for the full image $256 \times 256 \times 256$. For each value of the incident angle, the position of the laser spot on the screen was determined by computing its center of gravity (see Section 3.3). The 50 points of the deflection function shown in Fig. 4 were measured in a few minutes.

All effects likely to have an influence at the level of accuracy required (few $10^{-4}$ on $n$) had to be taken into account. In particular, distance measurements for the deviation angle determination were done carefully. Corrections to account for the Rayleigh scattering effects of the tile were also included (see Appendix A). See Refs. [22,23] for other measurements.

### 3.3. Results and discussion

A few tiles have been thoroughly studied using the prism method, scanning different laser beam entry positions across the tile thickness, at each of the four corners, for different positions along the eight edges, and for several distances from the edge along each of the four tiles sides.

The position of the laser spot on the screen could be determined by fitting the measured intensity distribution $I(x, y)$ with a 2D Gaussian shape, or the $X$ and $Y$ projections of the same with a 1D Gaussian, or by determining the center of gravity of the spot. The three methods gave very similar results, providing the position of the spot with an accuracy of the order of 0.1 mm, for spots of reasonable optical quality, as it was the case for most of the measurements performed with the red laser. In some cases, however, the poor surface quality led to distortion and a widening of the beam intensity distribution, thus degrading considerably the accuracy in the determination of the spot position. An example of the measured beam profile and its 2D Gaussian fit are displayed in Fig. 3. Various fitting procedures were tried to extract the refractive index, all based on relation (3). Some typical results are displayed in Fig. 4, showing the deviation $\delta$ as a function of the $\theta$ angle, with $\theta = \alpha - \pi/4$.

A significant difficulty arose for the measurements along the edges, since the prism angle $\beta$ could be different from its nominal value 90 by one degree or more for some tiles (no reliable method could be found to measure this angle accurately). In addition, the most suitable fitting procedure led to a strong correlation between prism angle and refractive index. This is mostly due to the value of $\beta$ being essentially determined by the branches of the curve $\delta(\alpha)$ away from the minimum, and its precise determination would have probably required a wider range of incident angle measured. This could not be performed in a simple way with the set-up configuration used for the measurements.

Fig. 5 illustrates the results with a typical index distribution measured in a narrow range along the edges of a sample tile (see also Fig. 10 further below). A clear edge effect is systematically observed, with the index value increasing towards the edges, and becoming even stronger close to the corners, by $\delta n \approx 10^{-3}$ or more.

A main observation of this study is then that the measured index varies much beyond the requirements over the narrow band along the edges accessible to measurements. These variations are along directions normal to the tiles edges. This is a general common feature observed for the AMS detector tiles (NOVO). This situation pointed to the need of a method allowing to investigate the index in the inner part of the tiles area. Further details can be found in internal notes [24,27].

## 4. Measurements in beam test

In the search for a suitable characterization procedure, the 500 MeV high optical quality Frascati electron beam was used in combination with the dedicated APACHE imaging system based on a spherical mirror focusing on a photographic emulsion plate, developed by the LHCb-RICH Milano team that hosted this test. See Ref. [28] for details on the experimental set-up. Two tiles could be studied in a run unfortunately shortened by technical accelerator problems.

An example of the measured rings is shown in Fig. 6. Only a part of the aerogel Cherenkov ring was detected, because of the larger index of the tested tiles ($n = 1.05$), than for the LHCb tiles

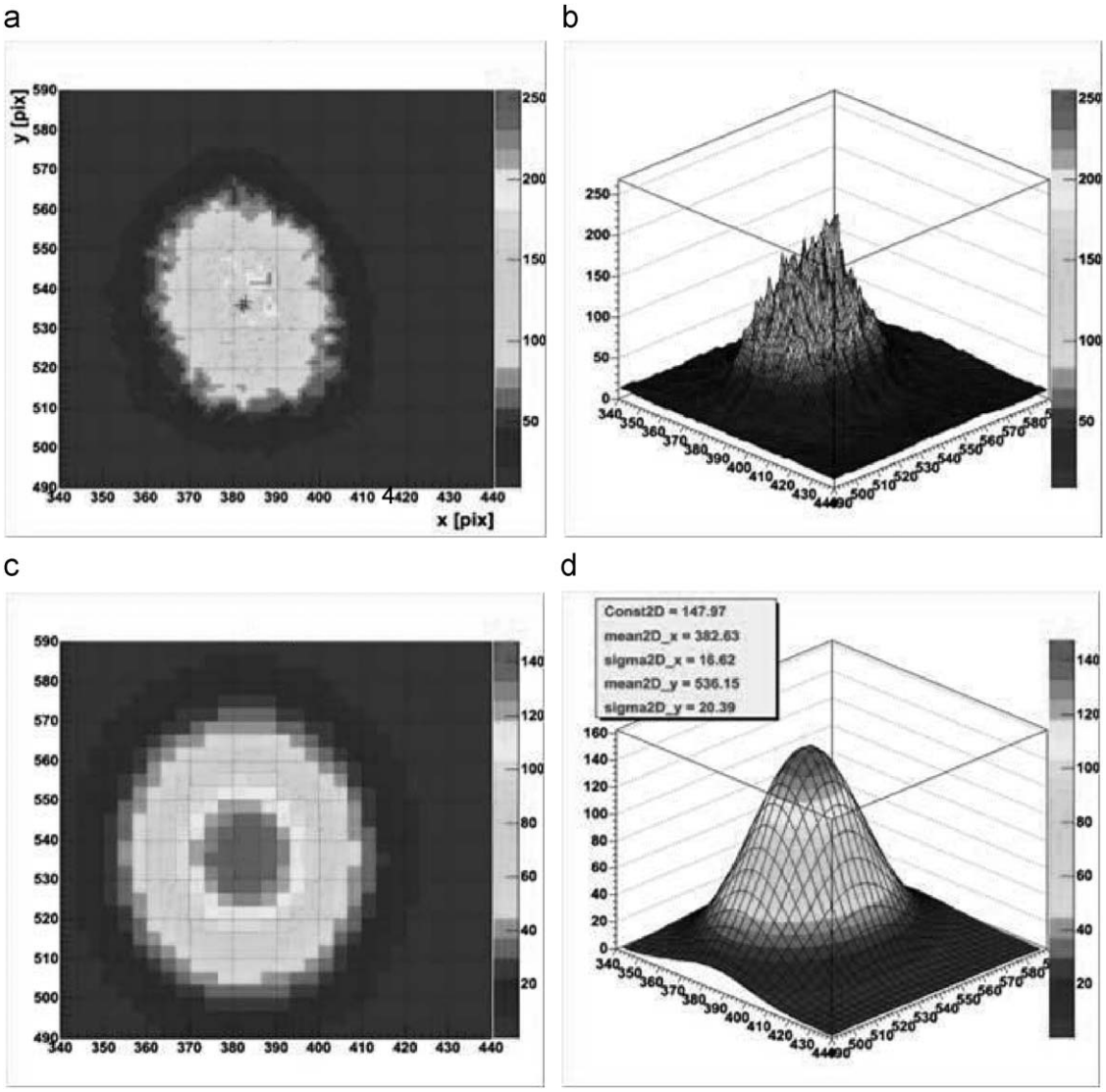


**Fig. 3.** Example of a measured image produced on the screen by the red laser beam refracted in the studied tile, and Gaussian shape used for fitting the experimental shape. The pixel size is about 0.15 mm. Top: 2D (left) and 3D (right) display of a laser beam spot. Bottom: 2D and 3D display of the resulting Gaussian fit.

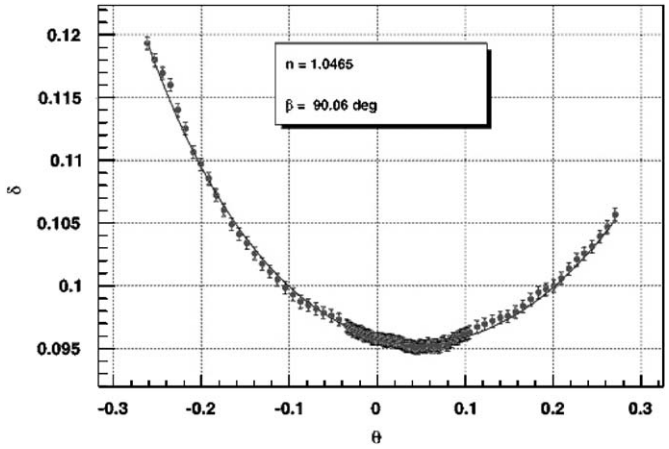


**Fig. 4.** Results obtained from fitting $n$ and $\beta$ in relation (3).

($n=1.03$). This significantly reduced the accuracy of the measurement. The smaller nitrogen ring generated by the beam in the drift space between tile mirror was also detected, while photons generated upstream were stopped with an absorber. The analysis procedure is detailed in Ref. [28]. An example of Cherenkov angle distribution for aerogel and nitrogen is displayed on the right hand side of Fig. 6. The tile surface is scanned over about 30 points, and such an angle distribution is reconstructed for each position. Fig. 7 represents the map of refractive index variation measured for the two aerogel tiles tested. The errors are estimated to be of the order of $\pm 3\times10^{-4}$ (see Ref. [27] for details). Three full days of beam time were needed to scan two tiles with a few tens of points each. This procedure is powerful and highly accurate (in optimum conditions), but extremely heavy and time consuming. It turned out finally not to be appropriate for the present purpose that required flexibility and rapidity of processing for characterizing several hundred tiles.

However, the test did confirm the variation of the index over the tile surface by about $\delta n=10^{-3}$ confirming the need of index mapping of the whole tiles area to match the accuracy requirements.

The tiles from both manufacturers were also tested in (low resolution) beams at CERN with their respective imager prototypes. The results can be found in Refs. [17,6] for the AMS and CREAM projects, respectively.

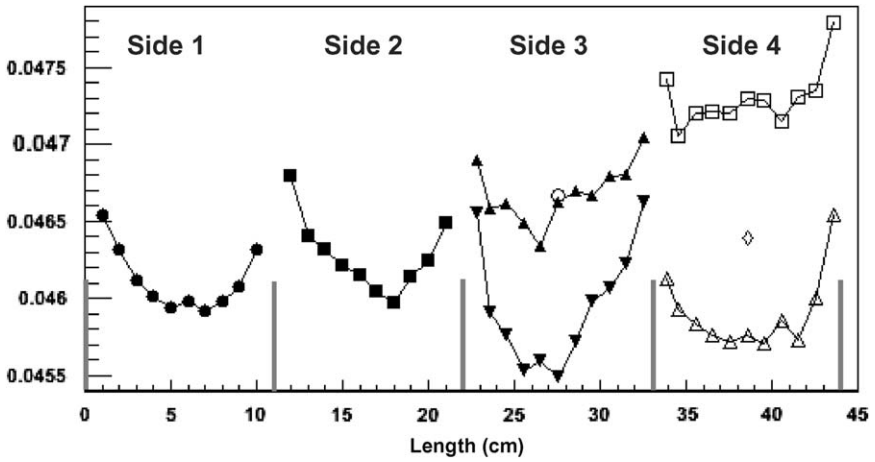


**Fig. 5.** Values of ($n$-1) measured along the edges of a sample tile. The ascissa gives the position along each of the four 11 cm long edges. The two sets of values along edges 3 and 4 (from the left) correspond to two different distances of entry point of the laser beam, close to the edge (3 mm) and around mid-thickness. Note the increasing values of the index close to the corners, and the significant differences between the values obtained at different distances from the edges.

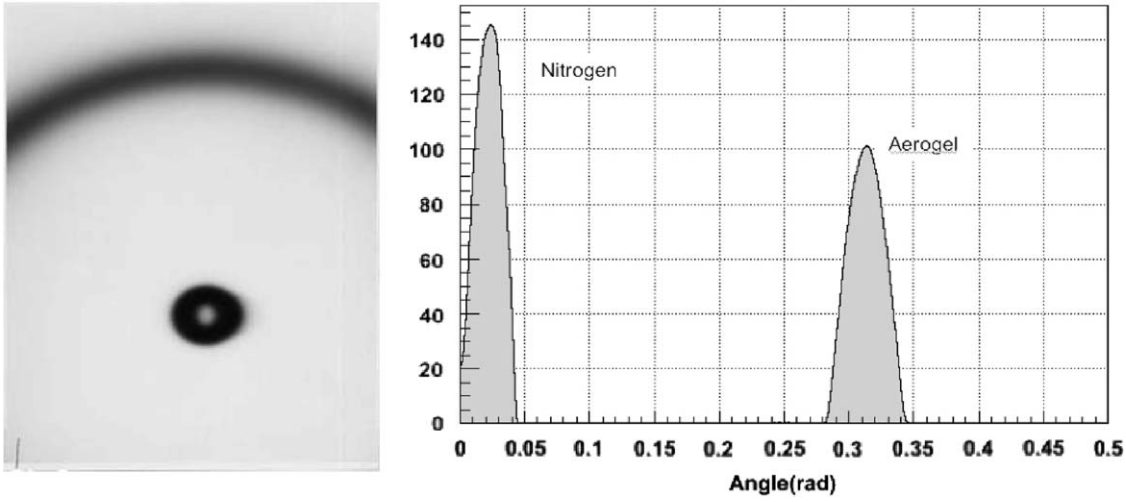


**Fig. 6.** Example of measured photons ring (left) and of Cherenkov angle distributions from aerogel and nitrogen (right).

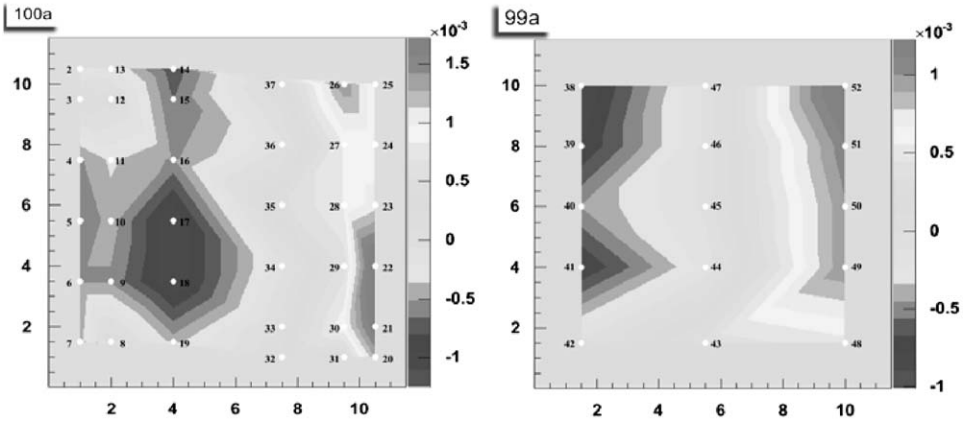


**Fig. 7.** Refractive index variations measured for the two aerogel tiles tested. Errors are $\pm 3 \times 10^{-4}$.

## 5. Gradient method

The measurements performed by the prism method and in the beam test have shown that the tiles suffer a large refractive index nonuniformity. A partial peripheral scan of the tile surface was considered not enough to reach the accuracy required for the detector performance aimed at.

The other method used to match the need of a larger coverage of the tiles area is based on the deviation of a light ray by the transverse gradient of index along its optical path. This is a well

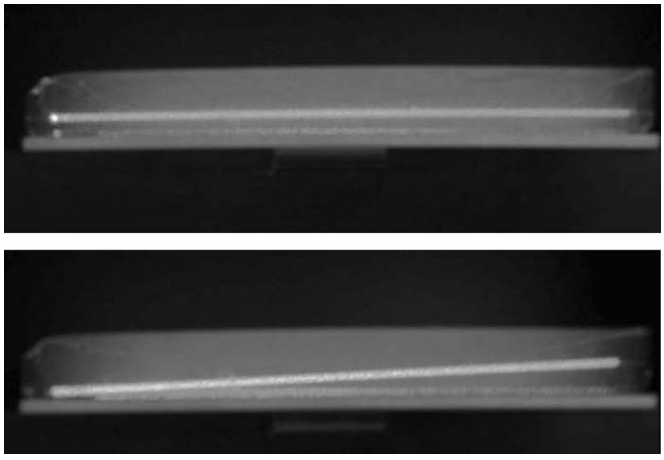

**Fig. 8.** Example of laser beam deflected by a gradient of refractive index across its thickness (Matsushita/Panasonic SP50 tile). Top: the beam enters from the left, normal to the side face, at mid-height of the tile. It is not deflected. Bottom: the beam enters very close to the lower face of the tile. It is progressively deflected along its path by the gradient of index close to the surface, until it reaches the region of constant index value where its path straightens up. The deflection angle is around 5°.

known effect also known to generate spectacular visual phenomena such as mirages. It is described in many textbooks (see Ref. [29] for example). For aerogel testing it was first proposed in Ref. [30], and it has been used recently in Ref. [28]. Its application to the present study is described below.

Fig. 8 illustrates the phenomenon with the example of an aerogel tile that was observed to have a significant gradient of index normal to the main faces and close to one of them.

### 5.1. Principle of the method

The principle of the method is illustrated in Fig. 9. A laser beam enters the tile normally to its surface for different positions. In the absence of transverse gradient of refractive index, there is no deviation. If a transverse gradient of refractive index, i.e. normal to the beam, is present, then the beam is deflected by normal (continuous) refraction effect. The measurement of the laser beam deviation provides a measurement of the index gradient along the crossed path. The mapping of the tiles surface using this technique could then provide a map of the refraction index averaged over the tile thickness.

The index gradient map can be reconstructed from the from the 2D experimental beam deviation map

$$\left(\frac{\Delta n}{\Delta x, \Delta n\, \Delta y}\right)$$

assuming a first order index variation from the neighboring experimental points.

Because of the experimental errors, the measured variations are not exact differentials, and the index reconstructed at point $(x,y)$ depends on its neighbors chosen for the reconstruction. To overcome this difficulty, the gradient map is obtained by minimization of a $\chi^2$ function defined by

$$\chi^2 = \sum_i \sum_{j\in neighbors} (n_i - \tilde{n}_i^j)^2 \quad (4)$$

where $\tilde{n}_i^j$ is the refractive index at point $i$, computed from the values of its nearest neighbors as $\tilde{n}_i^j = n_j + (\Delta n/\Delta x)(x_i - x_j) + (\Delta n/\Delta y)(y_i - y_j)$. The $\chi^2$ minimization provides a set of refraction index values $\{n_i\}$ in each point of the tile surface.

This measurement procedure, however, suffers a parasitic refraction effect. It is due to local, macroscopic, variations of the tile surface angle with the respect to the normal (beam direction). These angular variations induce corresponding refraction effects at the entrance and exit interfaces that can be of the same order of magnitude as the studied effect, and that could bias the results. Fortunately all the tiles turned out to have a flat face (likely corresponding to the mold floor at the production stage) and the problem was simplified. The tiles thickness had then to be carefully mapped to correct this effect. This was achieved by means of a high accuracy mechanical comparator.

The measurements could thus been corrected for each measurement point in the analysis. This is illustrated in Fig. 10.

This method, since relying on integration of the local gradient, provides only relative variations of the index value. The mean absolute value can be obtained the empirical from the empirical (Lorentz–Lorenz based) relation between the refractive index and the material density, deduced from the tiles weight and volume measurements. For a laser wavelength of 632.8 nm the relations used are

$$n^2 = 1 + 0.421\rho \quad \text{for NOV tiles [31]} \quad (5)$$

$$n = 1 + 0.26\rho \quad \text{for MATS tiles [32].} \quad (6)$$

In the case of hydrophilic aerogel, the weight of the sample was found to depend to a significant extent on the ambient atmospheric hygrometry and to vary on the scale of a percent. The weighting and the subsequent measurements had then to be performed for tiles stored in a dry atmosphere.

### 5.2. Experimental set-up

The set-up used for the measurements was the same as used for the previous measurements and described previously. In order to ensure the beam enters the tile normally to its surface with a sufficient accuracy, a dedicated alignment device has been designed, based on a prism system with reflecting mirrors, allowing a precision better than one tenth of a degree.

The tile scans were performed with 400 measurement points (20 in each of the two directions).

### 5.3. Results

A representative profile of measured refractive index is displayed in Fig. 10. As estimated by the two previous characterization methods tested (prism method and beam test), the mean nonuniformity of the refractive index in a each tile as measured over the whole batch, is of the order of $10^{-3}$. The measured maps will be taken used in the Cherenkov detectors simulations and in the subsequent data analysis, to correct for index gradient from tile to tile, and inside each tile.

### 5.4. Comparison of the two methods

The two methods, prism and gradient, can be compared over the ranges where both can be applied, i.e., along the edges of the tile. They were found to give consistently close results. This is illustrated on Fig. 11 where the value of $(n-1)\times 10^3$ obtained by the prism method and by the gradient method, respectively, are shown to be in pretty good agreement.

### 5.5. Other measurements methods

Other methods have been used in the literature. They are quoted here for completeness. Measurements of beam spot excursion induced by the parallel plate technique have been performed in Ref. [33], but the obtained results are not consistent

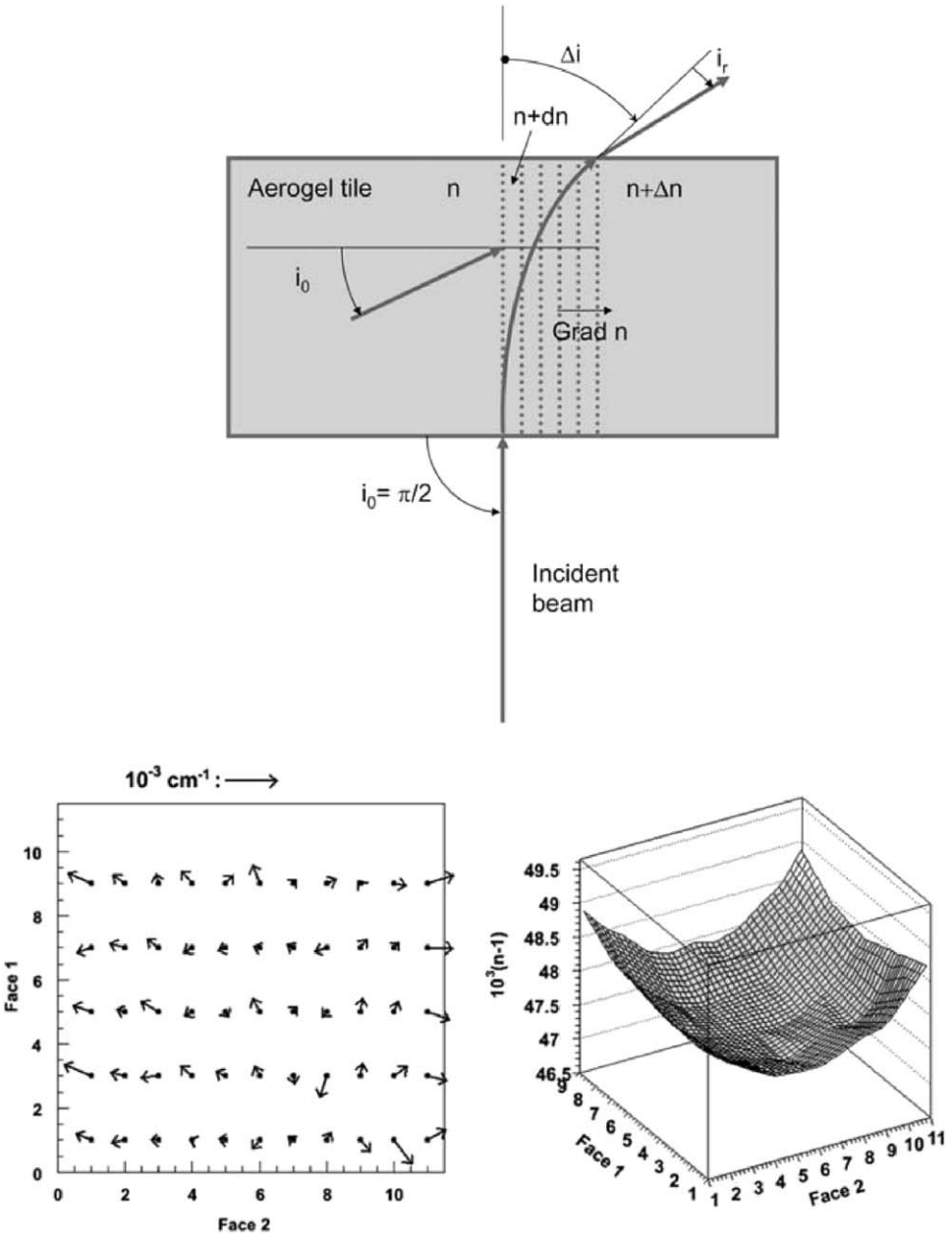


**Fig. 9.** Schematics of the gradient method principle (top). The bottom plot shows the example of a gradient map measured on a $11 \times 5$ grid. The arrow attached to each measured point gives the direction of the gradient, while its modulus provides the absolute value.

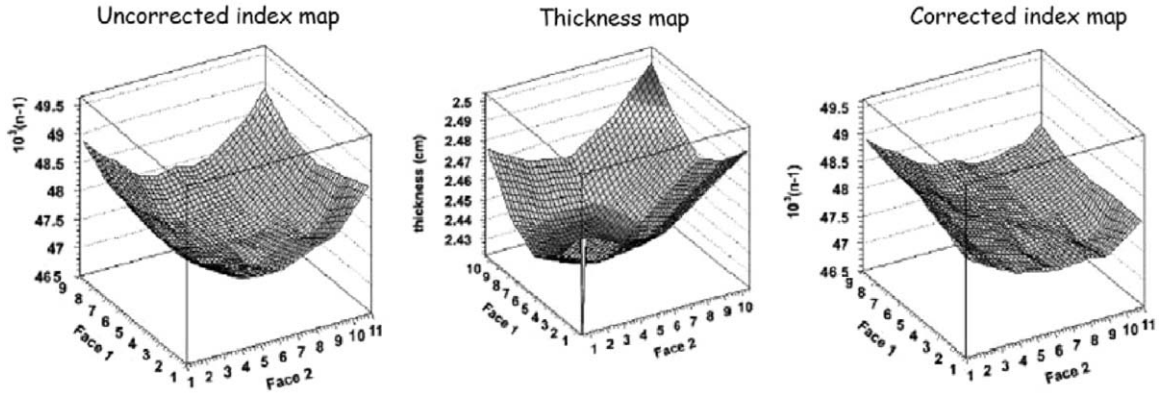


**Fig. 10.** Example of results obtained with a NOVO tile: uncorrected reconstructed index (left), thickness mapping (center), and corrected index map (right). Note the scale of variation of the thickness, of the order of 0.3–0.5 mm, and the changes induced on the final results with respect to the uncorrected index map.

with those found in other works. This technique suffers from a lack of accuracy. The powerful and highly accurate interferometry technique could also be considered [30]. However, the thickness of the sample has to be known to within a fraction of wavelength. Thickness control there, is a major hindrance that made the technique not applicable in the present project.

## 6. Results

It was found in the study by means of a simple simulation that combining the two methods would lead to an accuracy close to the targeted value of $1.5 \times 10^{-4}$ on the refractive index measurement for the NOVO tiles. However, the complete processing would have taken about half a day of work per tile in the best case, not including the data analysis, with basically 200 tiles to be processed for the AMS imager, and as many for the CREAM imager. The total amount of required time was not compatible with the construction and delivery schedule of the detectors, and the procedure had to be simplified and the accuracy requirement relaxed by a margin compatible with the counters resolution performances. Finally the measurement procedure applied was as described below for each set of tiles.

### 6.1. Novosibirsk production for the AMS imager

For the AMS imager, the mean index was obtained from the tiles weight and volume measurements in controlled hygrometric conditions (see Section 6.1), and all the tiles were optically scanned for gradient of index measurements. The resulting accuracy obtained for the local index values is estimated to $4 \times 10^{-4}$.

Fig. 12 shows the distributions of the mean refractive index and of the index dispersion inside each tile, over the whole batch of available tiles.

### 6.2. Matsushita–Panasonic production for the CREAM imager

The CREAM Cherenkov imager radiator plane consists of 200 tiles, plus 13 spares. The index accuracy required for this detector was less stringent than for AMS. Since the optical mapping of a significant sample of tiles showed a high transverse (parallel to the main faces) index uniformity for the whole set of tiles, it was admitted that a systematic optical scanning was not necessary. The tiles were weighted and thickness mapped. The mean index was evaluated by relation (6). The thickness mapping showed that

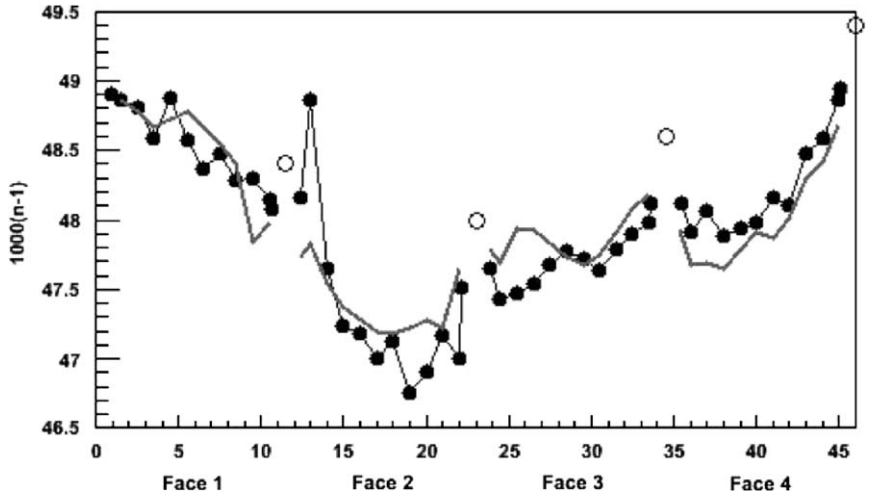


**Fig. 11.** Comparison of the results obtained by the two methods for a sample tile. The full circles are the data points measured by the prism method along the tile edges (vertical tile position). The open circles are from the measurements on the four corners (horizontal tile position) the black line between the points being to guide the eye. The gray line corresponds to the measurements from the index gradient method extrapolated to the tile edge. The position along the sides (bottom scale) are in cm.

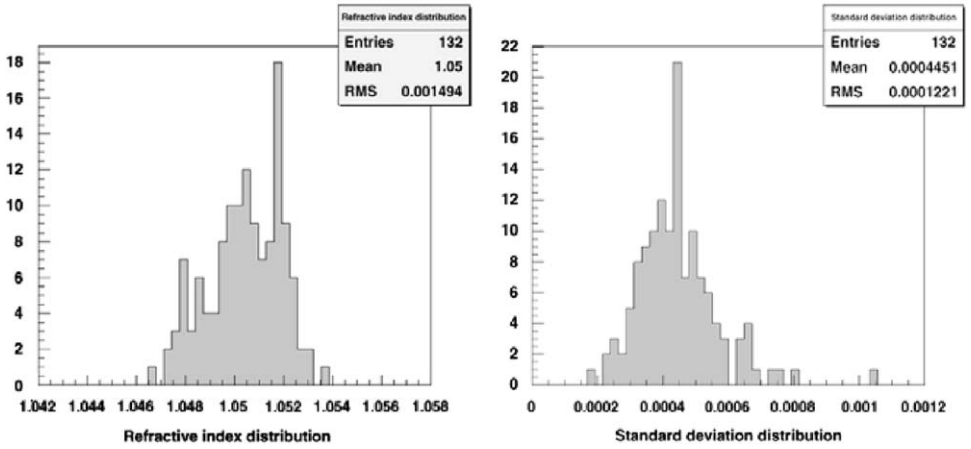


**Fig. 12.** Left: mean refractive index $\langle n \rangle$ distribution obtained from 132 AMS radiator tiles (92 nominals plus 40 spares). Right: distribution of the index spread per tile $\sigma_n$ (rms) from the same sample.

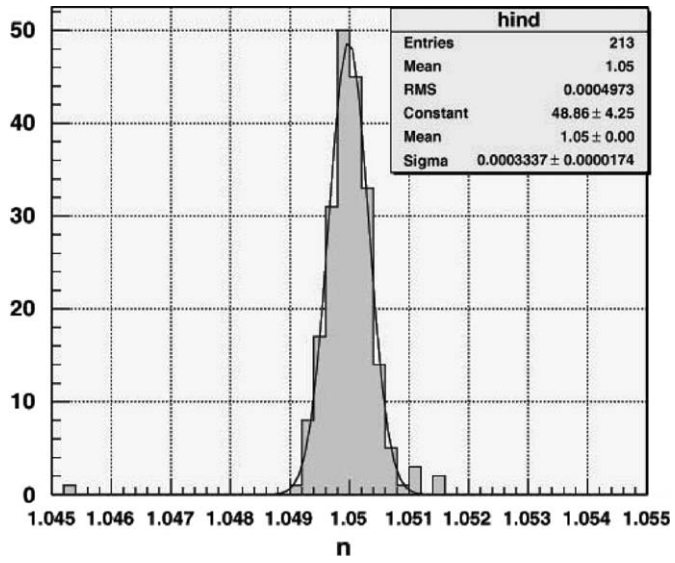


**Fig. 13.** Mean index distribution of the SP50 batch of tiles for the CREAM imager. Note the small spread (standard deviation $\sigma \sim 3.3 \times 10^{-4}$) of the distribution, matching the Chercam design requirements.

most units had a thickness varying slowly by a fraction of a millimeter across the main dimension of the tile, along a diagonal or along a side. The radiator thickness for the detector is 22 mm, and the tiles (11 mm thick) had to be paired. The appropriate sorting and pairing for index value and geometrical orientation for the stack to have an optimized thickness uniformity (see section below), was performed by means of a dedicated software [24]. It lead to a thickness of the set of two-tiles stacks brought from a natural individual tile thickness $t$ spread $\sigma_t \approx 0.3$ mm, down to $\sigma_t \approx 0.1$ mm for the matched pairs, thereby matching the height uniformity requirement for of the radiator plane of 0.2 mm (see Section 2.3).

The refractive index distribution obtained as mentioned above, for the whole set of tiles (production+spare) is displayed in Fig. 13.

The clarity coefficient of these tiles has been measured at the Madrid CIEMAT laboratory on a sample of four tiles, with a good accuracy by means of a refractometer. The values measured are all within the range $15-17 \times 10^{-3}$ μm$^4$/cm, which is significantly worse than mentioned by the provider.

## 7. Other features of silica aerogel

In order to ensure the accuracy level of a few $10^{-4}$ on the measurement, the study was completed with measurements of the pressure dependence of the refractive index, and of its dependence on the hygrophilicity, for the AMS tiles. An indication on the aging properties of the material, and on some anomalous results are also reported.

### 7.1. Pressure dependence

The refractive index measurements were performed under atmospheric pressure, which is not the working conditions of the Cherenkov imager in orbit. A series of measurements have therefore been performed to evaluate the pressure dependence of the refractive index. A dedicated set-up was used, in which a He–Ne laser beam was refracted by a sample tile placed in a controlled pressure vessel. The pressure was varied from $10^{-7}$ to 1 atm. The measurements were performed 5 m downstream on 20 points of the deflected beam spot. The pressure cycle was repeated several times, from low to high pressure and vice versa, with no significant variation observed between the different measurements. The maximum variation amplitude of the spot position observed was around 0.5 mm, corresponding to a deviation angle $\Delta\delta \approx 10^{-5} \approx 2\Delta n/n$ with $n = n_{AGL}/n_{air}$. This corresponds to an index variation of $3.5 \times 10^{-4}$. The same result is obtained by calculating $\Delta n$ from the density variation using the Young modulus of the aerogel provided by the manufacturer, $E = 50$ MPa. Such a small excursion of the mean index induced by the pressure difference between pressure on the ground and in orbit, will not have any other consequence on the detector performances than a very small correction of the nominal values of the mean index in the data analysis.

### 7.2. Temperature dependence

The thermal expansion coefficient of the aerogel being very small (around $4 \times 10^{-6}\,K^{-1}$) [25], only small variations are expected on large temperature scales. For a 40 °C temperature variation, the expected refractive index variation is $\Delta n_{AGL}/n_{AGL} \approx 2 \times 10^{-6}$, a totally negligible effect in the present case.

### 7.3. Evolution of hydrophilic tiles

As previously mentioned, the Novosibirsk tiles, equipping the AMS radiator plane, are hydrophilic. Their properties, in particular mass and density are thus expected to vary over time with the humidity level of the ambient atmosphere. This is illustrated in Fig. 14, showing the measured time dependence of a sample tile weight after it has been taken out of its dry storage and put in open air with natural ($\approx 60\%$) humidity. The weight variation is at the percent level, and so is the associated variation of $(n-1)$, corresponding to an index variation $\Delta n \sim 5 \times 10^{-4}$, of the order of the experimental accuracy limit for the AMS imager. See also Ref. [26]. Dry atmosphere conditions had then to be applied as much as possible, for the measurements, to avoid this effect.

The tiles were stored in an air-tight lucite box under monitored dry nitrogen atmosphere provided by a controlled flow from a large volume cryostatic $N_2$ storage tank. The humidity was monitored and kept below $\sim 25\%$.

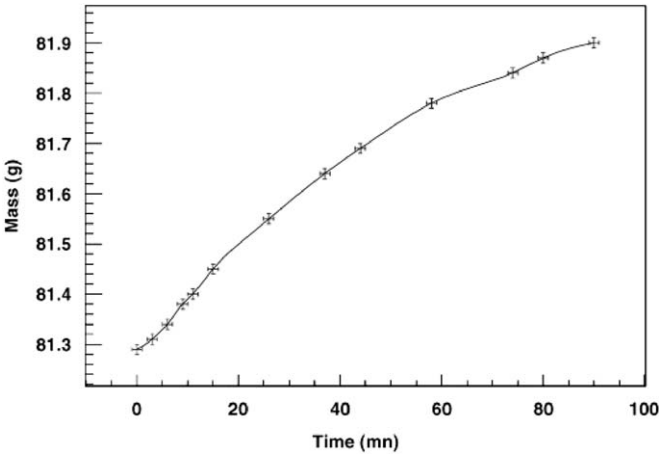


**Fig. 14.** Time dependence of the weight of a hydrophilic tile from the time it is taken out of its dry storage atmosphere.

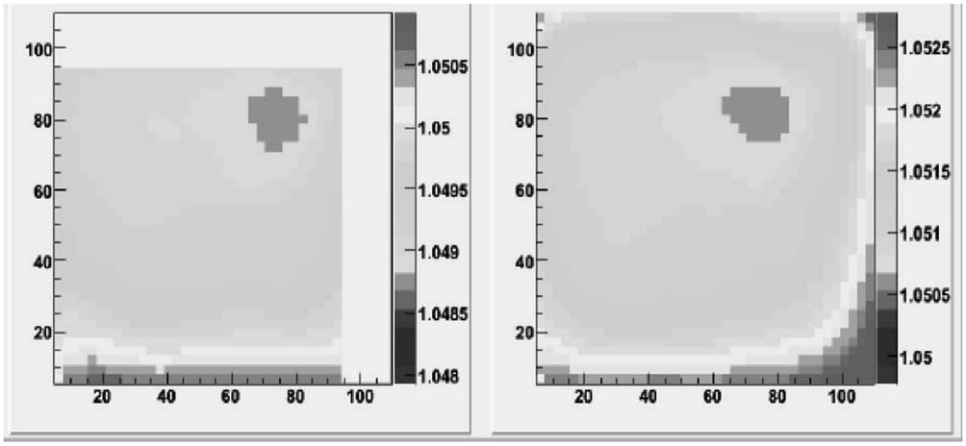


**Fig. 15.** Comparison of measurements performed at one year interval, on 2006 (left) and 2007 (right). A fraction of the tile area was not covered in the 2006 measurement, because of the experimental set-up arrangement. This was changed later to allow scanning the whole tile area.

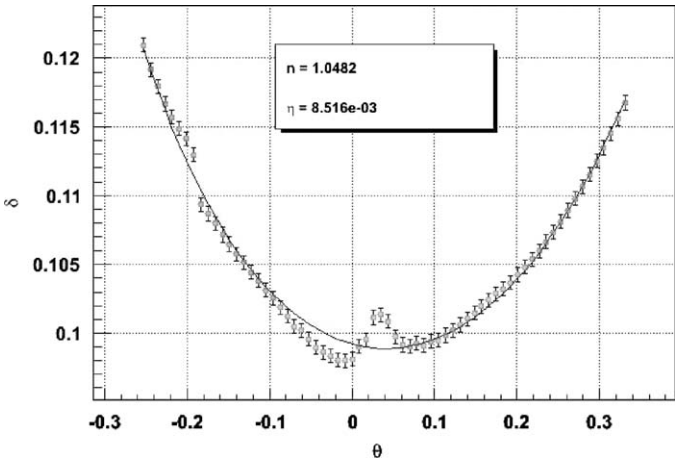


**Fig. 16.** Anomalous angular distribution observed for one of the 200 tiles characterized in the study.

### 7.4. Long term stability

An indication on the evolution of the tiles optical properties could be obtained on a longer time range with a tile tested twice at a one year interval. The comparison can be seen in Fig. 15. Some significant variations of the mean index are observed, likely because of the different atmosphere hygrometric conditions, but the overall map profiles remained very similar.

### 7.5. Anomalous deflection function:

Fig. 16 shows an anomalous deflection function measured on a particular NOVO tile with the prism method. The whole set of 11 angular distributions measured along the 11 cm of the edge showed the same feature. The origin of this anomaly is not understood.

## 8. Summary and conclusion

Two productions of silica aerogel tiles from two different providers for the Cherenkov imagers of the AMS and CREAM experiments, have been systematically studied and characterized with the purpose of reaching an accuracy of the order of $1.5\times10^{-4}$ on the refractive index measurement. The study showed that such a requirement could be met only at the price of a heavy metrological effort, by combining two complementary measurement methods. For both detectors, a specific compromise taking into account material features and accuracy requirements, had to be made and a simplified procedure adapted leading to less accurate measurements but still acceptable for the scientific program.

For the AMS imager, more than 200 tiles were optically scanned for index variations mapping. Their weight and dimension (thickness map) measurements, provided their mean index values completing their detailed index map. The developed procedure allowed to reach an accuracy on the refractive index determination of $4\times10^{-4}$, compatible with the AMS science project. This accuracy is close enough to the required value to allow isotope separation of light nuclei up to around 10 GeV/$c$ momentum in AMS.

For the CREAM imager, the accuracy requirement on the refractive index was less stringent than for AMS, a complete optical mapping was not necessary, but the same weight and dimension measurements were performed on the set of more 200 tiles. The rms value of the obtained refractive index distribution, of $3\times10^{-4}$, was comfortably within the requirements for this detector.

Some other features of the aerogel tiles relevant to the counter performances were also investigated, such as the pressure dependence of the index and its hygrometric sensitivity.

In-flight calibrations should provide a cross check of the mean values of the refractive index for each set of tiles measured here.

The AMS Cherenkov imager was integrated in 2008. It is currently under ground tests at CERN. The experiment is scheduled for launch on September 2010.

The CREAM Cherenkov imager was built in 2006, integrated in 2007, and flown on December of the same year, taking significant data that are currently being processed [34]. The detector was flown again on last December 2008 and January 2009 in similar conditions. It is scheduled to fly again on next winter 2009–2010.

## Acknowledgments

The authors are grateful to the Budker and Boreskov laboratories scientists, especially A. Danilyuk, E. Kravtchenko, and A. Onuchin, for their help in this work. They thank J. Casaus and J. Berdugo, for performing the clarity coefficient measurements of the SP50 tiles samples in CIEMAT Madrid. They are much

indebted to the LPSC technicians, J.P. Scordilis and M. Marton, whose constant help in this work was invaluable, and to G. Michel and the workshop team for their constant availability on many mechanical works on the project. A. Barrau, M. Buénerd, L. Derome and K. Protasov acknowledge partial support from the INTAS program 03-52-5579. This work has been partly funded by the ANR Project ANR-06-BLAN-0042. The Mexico UNAM authors acknowledge financial support from CONACYT, DGAPA-UNAM, and HELEN Projects.

## Appendix A. Clarity correction

This effect is induced by the different path lengths crossed inside the material by the incident beam rays, due to the transverse extension of the beam. Because of these differences, the rays undergo different attenuations induced by Rayleigh scattering (light absorption being negligible), resulting in a small shift of the beam center of gravity that needs to be corrected for. Taking the beam intensity distribution in the deflection plane as

$$I_0(x)=\frac{1}{\sqrt{2\pi}\sigma}e^{-(x-x_0)^2/2\sigma^2}.$$

The optical path difference between the central ray and the ray at transverse distance $x_1$ (see Fig. A.1 for notations) is

$$\Delta p = x_1\tan\alpha - \frac{\sin\beta}{\sin\left(\frac{\pi}{2}-\beta+\alpha_2\right)\cos\alpha}x_1 + x_1(\tan\alpha_4-\tan\delta)$$

$$\alpha_2=\arcsin\frac{\sin\alpha}{n}.$$

$p$ being the path length of the optical rays. The first term is the path difference before the sample (aerogel tile here), the second one is the path difference inside the tile, and the third one between tile and screen. Only the second one matters for the clarity correction:

$$\Delta p_{agl}=\frac{\sin\beta}{\sin\left(\frac{\pi}{2}-\beta+\arcsin\frac{\sin\alpha}{n}\right)\cos\alpha}x_1=Dx_1.$$

The wavelength dependence of the aerogel transmittance for silica aerogel depends to a good approximation only on Rayleigh scattering, namely

$$A(d)=A_0e^{-Cd/\lambda^4}$$

where $d$ is the thickness crossed by the beam, and the clarity $C$ is proportional to the inverse scattering length: $C\sim 1/L_{scat}$. And a ray passing at a distance $|x-x_0|$ off the beam center will be attenuated compared to the central intensity by a factor $A(x)$ (i.e. $I(x)=I_0(x)A(x)$) with

$$A(x)=A_0e^{-(C/\lambda^4)D(x-x_0)}.$$

The intensity in $x$ then becomes

$$I(x)=\frac{1}{\sqrt{2\pi}\sigma}\,e^{-(C/\lambda^4)D(x-x_0)-(x-x_0)^2/2\sigma^2}=\frac{1}{\sqrt{2\pi}\sigma}\,e^{-(x-x_1)^2/2\sigma^2}\,e^{C^2D^2\sigma^2/2\lambda^8}.$$

With $x_1=x_0-CD\sigma^2/\lambda^4$. The beam asymmetrically damped, and the beam centroid thus shifted. With $L=3$ m, $x_0=30$ cm, $\beta=\pi/2$, $n=1.05$, $\alpha=\alpha_{min}\approx 0.84$ rad and $l'\approx 1$ cm, $C=0.0051\,\mu\text{m}^4\,\text{cm}^{-1}$ and $\sigma=3$ mm, the shift is of the order of $x_0-x_1\approx 0.25$ mm.

For these values,

$$D=\frac{\sin\beta}{\sin\left(\frac{\pi}{2}-\beta+\arcsin\frac{\sin\alpha}{n}\right)\cos\alpha}\approx 1.4938.$$

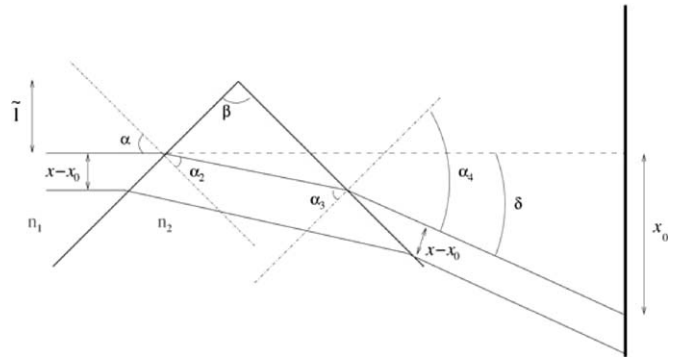


**Fig. A.1.** Notations used for clarity corrections.

## References

[1] D.E. Fields, et al., Nucl. Instr. and Meth. A 349 (1994) 431.
[2] T. Matsumoto, et al., Nucl. Instr. and Meth. A 521 (2004) 367.
[3] T. Bellunato, et al., Nucl. Phys. B (Proc. Suppl.) 150 (2006) 281.
[4] Y. Asazoka, Nucl. Instr. Meth. A 416 (1998) 236.
[5] F. Baraõ, The AMS collaboration, in: Proceedings of the International Conference on Cosmic Rays (ICRC) 2007, Merida, Mexico; F. Baraõ, et al., in: Proceedings of the 5th International Workshop on New Worlds in Astroparticle Physics, Faro, Portugal 2005, World Scientific.
[6] L. Derome, et al., in: International Conference on Cosmic Ray Physics (ICRC) 2007; Y. Sallaz-Damaz, in: 6th International Workshshop on Ring Imaging Cherenkov Counters, Trieste, Italy, October 15–20, 2007, Nucl. Inst. and Meth. in Phys. Res. A 595 (2008) 62; M. Mangin-Brinet et al, Nucl. Instr. and Meth. A 572, (2007) 410.
[7] M. Tabata, et al., in: Proceedings of the Nuclear Science Symposium IEEE 2005, vol. 2, October 2005, p. 816; Y. Ishii, et al., in: Proceedings of the Nuclear Science Symposium IEEE, vol. 1, October 26, 2007, p. 663.
[8] N. Akopov, et al., Nucl. Instr. and Meth. A 479 (2002) 511;
H.E. Jackson, Nucl. Instr. and Phys. Res. A 553 (2005) 205.
[9] I. Adachi, et al., Nucl. Instr. and Meth. A 553 (2005) 146;
I. Adachi, et al., Nucl. Instr. and Meth. A 595 (2008) 80;
T. Ijima, et al., Nucl. Instr. and Meth. A 548 (2005) 583;
A.Yu. Barnyakov, et al., Nucl. Instr. and Meth. A 553 (2005) 70.
[10] A.Yu. Barnakov, et al., Nucl. Instr. and Meth. A 553 (2005) 125;
A.Yu. Barnakov, et al., Nucl. Instr. and Meth. A 494 (2002) 491.
[11] I. Adachi, et al., Nucl. Instr. and Meth. A 355 (1995) 390;
H. Yokogawa, M. Yokoyama, J. Non-cryst. Solids 186 (1995) 23.
[12] Matsushita-Panasonic Electric Works, Ltd., 1048 Kadoma, Osaka, Japan ⟨http://www.mew.co.jp/e-aerogel⟩.
[13] A. Danyliuk, Boreskov Catalysis Institute of Novosobirsk, private communication.
[14] ⟨http://ams.cern.ch/AMS/ams_homepage.html⟩.
[15] ⟨http://cosmicray.umd.edu/cream/cream.html⟩.
[16] E. Kravtechenko, A. Onuchin, Budker Institute of Novosobirsk, private communication.
[17] P. Aguayo, et al., Nucl. Instr. and Meth. A 560 (2006) 291.
[18] M. Buénerd, Z. Ren, Nucl. Instr. and Meth. A 454 (2000) 476.
[19] see for example M. Born, E. Wolf, Principles of Optics, sixth ed., Pergamon Press, Oxford 1980.
[20] M. Vargas-Trevino, Thesis, J. Fourier University, Grenoble, France, July 2005.
[21] see for example M. Born, A. Wolf, Principle of Optics, Pergamon Press, Oxford 1975.
[22] M. Villoro, et al., Nucl. Instr. and Meth. 480 (2002) 456.
[23] T. Bellunato, et al., Eur. Phys. J. C 52 (2007) 759.
[24] Y. Sallaz-Damaz, Ph.D. Thesis, Université J. Fourier, Grenoble, October 2008.
[25] J. Gross, J. Fricke, J. Non-cryst. Solids 186 (1995) 301.
[26] T. Bellunato, et al., Nucl. Instr. and Meth. 527 (2004) 319;
D.L. Perego, Nucl. Instr. and Meth. 595 (2008) 224.
[27] M. Mangin-Brinet, Diplôme d'Habilitation à Diriger les Recherches (DHDR), Université J. Fourier, November 2007.
[28] T. Bellunato, et al., Nucl. Instr. and Meth. A 556 (2006) 140.
[29] See for example W.J. Humphreys, Physics of the Air, third ed., McGraw-Hill, New York, 1940; ⟨http://mintaka.sdsu.edu/GF/mirages/mirintro.html⟩ for a recent source.
[30] L.W. Hrubesh, C.T. Alviso, in: Materials Research Society Symposium Proceedings, vol. 121, 1988, p. 703.
[31] A.F. Danilyuk, et al., Nucl. Instr. and Meth. A 494 (2002) 491.
[32] H. Yokogawa, Handbook of Sol–Gel Science and Technology, vol III, Kluwer, 2005, p. 73.
[33] D. Richter, D. Lipka, Nucl. Instr. and Meth. A 513 (2003) 635.
[34] L. Derome, et al., in: International Conference on Cosmic Rays (ICRC), Lódź, Poland, July 7–15, 2009.